

## Spectroscopy – A Powerful Diagnostic Tool in Source Development

U. Fantz\*, H. Falter, P. Franzen, S. Christ, B. Heinemann, A. Lorenz, W. Kraus, P. McNeely, R. Riedl, E. Speth, D. Wunderlich

*Max-Planck-Institut für Plasmaphysik, EURATOM Association, Boltzmannstr. 2, D-85748 Garching, Germany*

\*E-mail: fantz@ipp.mpg.de

### Abstract

Development of negative hydrogen ion sources for neutral beam systems is closely linked with an optimisation of negative ion formation in hydrogen plasmas which requires knowledge of the plasma parameters. Emission spectroscopy is introduced as a non-invasive and in-situ diagnostic tool for line of sight averaged plasma parameters. Diagnostic lines and simplified analysis methods for a variety of plasma parameters, such as electron density and electron temperature, gas temperature, atomic and molecular hydrogen density as well as cesium densities (atoms and ions) and negative ion densities are identified and prepared for direct application. Emphasis is laid on results obtained in RF generated negative ion sources. Correlations of plasma parameters with extracted negative ion current densities are discussed. Stripping losses in the extraction system are quantified by using beam emission spectroscopy.

### 1. Introduction

Heating and current drive of future magnetically confined fusion devices such as ITER requires neutral beam injection systems based on negative hydrogen ions ( $H^-$ ,  $D^-$ ) [1]. The requirements of high current densities over a large area coupled with long pulse operation have initiated a development program for negative ion sources. Here, two types of sources are investigated: the filamented arc source, KAMABOKO type, [2] and the RF source, developed at IPP Garching [3,4].

One of the main tasks in the development of negative ion sources is the optimisation of negative ion formation in the hydrogen plasma. The underlying reaction chain in the plasma volume is the dissociative attachment of vibrationally excited hydrogen molecules in the ground state:  $H_2(v) + e \rightarrow H_2^- \rightarrow H + H^-$ . For the destruction of negative ions with their binding energy of 0.75 eV two processes are dominant: the electron stripping ( $e + H^- \rightarrow 2e + H$ ) being very effective for electron temperatures ( $T_e$ ) in the range of a few eV, and the mutual neutralisation ( $H^+ + H^- \rightarrow H + H$ ) which depends slightly on ion temperature ( $T_i$ ). Electron stripping can be minimised by reducing  $T_e$  to approx. 1.5 eV, but then mutual neutralisation will take over. In either case this results in short survival lengths for the negative ions (cm range). As a consequence,  $H^-$  formation close to the extraction system of negative ion sources should be maximized. This demand can be fulfilled by a surface process, i.e. the interaction of atoms or ions with materials of low work function:  $H/H_x^+ + \text{surface } e^- \rightarrow H^-$ . Currently evaporation of cesium is used to cover the plasma grid of the extraction system with thin layers of cesium to lower the work function of the grid. It is obvious that such a complex plasma chemistry requires the knowledge of the plasma parameters which can then provide an insight in the underlying processes being useful for the optimisation of individual processes. Of particular interest is the plasma region close to the extraction area and diagnostic methods are essential which can provide a correlation of measured plasma quantities with extracted

current densities.

Among the variety of plasma diagnostic methods emission spectroscopy represents a passive, and therefore non-invasive, diagnostic tool with a simple and robust set-up. Spectra can be recorded easily with sufficient temporal resolution whereas several lines of sight provide spatial resolution. However, interpretation of spectra and quantification of plasma parameters might be quite complex in molecular low pressure plasmas [5,6].

An absolute calibration of the optical system offers the possibility to obtain a variety of different plasma parameters: electron density and electron temperature, gas temperature, atomic and molecular hydrogen densities as well as cesium densities (atoms and ions). In particular, monitoring of cesium emission reflects the cesium distribution inside the source by cesium evaporation and redistribution by the plasma itself, i.e. sputtering during the pulse. Furthermore, this diagnostics is also capable of deducing the most interesting parameter, namely the negative ion density.

A further diagnostic method is the  $H_{\alpha}$ -beam emission spectroscopy which allows a quantification of the stripping losses in the extraction system. Thus, comparisons with present model calculations can be carried out.

Emission spectroscopy is used as a routine diagnostic tool for the present RF sources at IPP. The experimental set-up, the spectroscopic systems, and the analysis methods will be introduced. Results for a variety of parameters will be shown and correlations of line intensities with extracted current densities of negative ions and electrons will be presented and discussed. Identical spectroscopic systems and same analysis methods are applied to the KAMABOKO arc source on the MANTIS testbed at CEA, Cadarache [7,8]. Some results will be discussed with focus on a comparison between the two types of sources.

## 2. Experimental set-up

### 2.1. RF ion source

The inductively coupled RF discharge ( $f = 1$  MHz,  $P_{\max} = 140$  kW) operates in the pressure range of 0.2 to 1 Pa. Figure 1 shows the principle design, details of the IPP RF source are given in [9,10]. The discharge chamber is separated into the driver region (cylinder,  $d \approx 20$  cm), where the plasma is generated, and the expansion region (rectangle). Close to the extraction system a magnetic filter field ( $B \approx 10$  mT) is applied to reduce the temperature of the electrons, and, thus, to reduce the destruction rate for  $H^{-}$  by electron stripping. The plasma parameters in this extraction region are typically:  $T_e \approx 3$  eV and  $n_e \approx 5 \times 10^{17} \text{ m}^{-3}$  whereas the driver plasma is characterised by  $T_e \approx 8$  eV and  $n_e \approx 5 \times 10^{18} \text{ m}^{-3}$ , both for hydrogen discharges with 120 kW input power and 0.6 Pa filling pressure. Cesium can be evaporated by an cesium oven mounted at the backplate of the rectangular body. The evaporation rate is adjusted empirically by the oven temperature.

At present two testbeds with almost identical sources are in operation at IPP: BATMAN (Bavarian Test Machine for Negative Ions) and MANITU (Multi Ampere Negative Ion Test Unit), for details see [3,4]. The main difference is the size of the extraction system. BATMAN operates with a small grid area ( $\approx 70 \text{ cm}^2$ , indicated in figure 1), in MANITU the area can be expanded up to  $300 \text{ cm}^2$ . MANITU is dedicated to long pulse operation, whereas standard discharges are usually limited to a pulse duration of 6 s.

### 2.2. Spectroscopic systems

Spectra are recorded with two types of spectrometers: a high resolution survey spectrometer

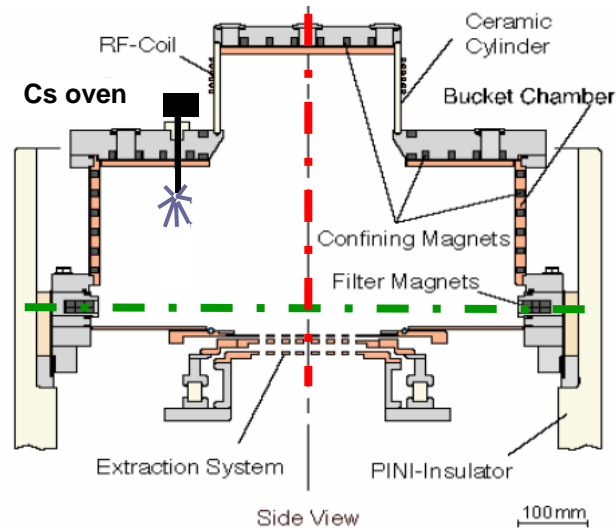


Figure 1. Schematic set-up of the RF ion source at the IPP with two lines of sight (broken lines) for spectroscopy: perpendicular to the grid ( $\perp$  grid) and parallel to the grid ( $\parallel$  grid).

(ESA2000,  $\Delta\lambda_{\text{FWHM}} = 20\text{-}35$  pm,  $\lambda = 200\text{-}750$  nm) and a low resolution survey spectrometer (S2000,  $\Delta\lambda_{\text{FWHM}} \approx 1\text{-}1.8$  nm,  $\lambda = 200\text{-}870$  nm). The high resolution survey spectrometer takes one spectrum at a fixed time during the discharge, whereas the low resolution survey spectrometer is capable of recording time traces, with a maximal time resolution of 5 ms. The optical fibres are equipped with collimator lenses such that a plasma volume with diameter 1 cm is imaged. All spectroscopic systems are absolutely calibrated by means of an Ulbricht sphere and a deuterium lamp. Due to their robust and compact construction they can be used flexible at the two testbeds; they have been also used for the measurements at the filamented KAMBOKO source at CEA (see section 5).

### 2.3. Temporal and spatial resolution

The two available low resolution survey spectrometers (S1 and S2) are suitable for plasma monitoring, i.e. they record time traces of several line integrals, which can be individually defined, in real-time observation. The resolution in time is correlated with the exposure time. Typical recording values are exposure times of some ten milliseconds at a fixed time interval of 100 ms for pulse lengths of the discharge being around 6 s. The high resolution survey spectrometer is limited in time resolution, due to the need of a large memory space for the CCD chip, and is adjusted to record one spectrum at 2 s after the begin of the pulse.

Diagnostic flanges with optical windows for emission spectroscopy are available in different locations. Lines of sight (LOS) are available through both the centre of the driver and expansion region onto the grid system (z-direction, red broken line in figure 1) and parallel to the grid (x- and y-direction, approximately 4 cm above the first grid, green broken line in figure 1). In BATMAN, additional flanges are attached in x-direction approximately 1.5 cm above the first grid. In BATMAN the grid contributes to  $\approx 20\%$  to the length of the LOS, whereas in MANITU the contribution is about 80% for the largest grid size.

Thus, in summary, three principle LOS are available for spatial information: one LOS  $\perp$  grid, and two LOS  $\parallel$  grid with 1.5 cm and 4 cm distance, respectively. Since emission is much higher in the driver than in the expansion region the line of sight averaged results obtained from the LOS  $\perp$  grid reflect the plasma parameters of the driver. In combination with the low resolution survey spectrometer time resolved spectra are obtained providing a resolution of 100 ms.

### 3. Diagnostics of plasma parameter

For diagnostics of plasma parameters using emission spectroscopy one can distinguish between several principle methods. The simplest one is the line identification in spectra. Besides expected emission lines of hydrogen and cesium, survey spectrometers are specially suited to detect impurities. Small water leaks or traces of air in the system are immediately recognized through OH, O, N<sub>2</sub> or N radiation. In addition, sputtering of wall material and arcing are readily observed. Furthermore, the transition from one gas species to another, e.g. from hydrogen discharges to deuterium discharges can be followed in the sequence of discharges by the decrease of the intensity ratio H<sub>β</sub>/D<sub>β</sub>. Recording the time traces of various emission lines during a discharge reflect gives access to the plasma dynamics.

Further steps in emission spectroscopy concern the quantification of measured radiation and correlation with plasma parameters, in particular particle densities. Common methods are line ratio measurements and analysis of absolute intensities together with population modelling. The following subsections discuss suitable diagnostic lines, analysis methods, and the corresponding results.

#### 3.1. Correlation of line intensities with plasma parameters

Measured line radiation gives, in a first step, information about the population of an electronically excited state. The relation with the ground state population, and thus with the particle density, is obtained from population models, so-called collisional radiative models which are available for atomic and molecular hydrogen, and for helium and argon gases, being used for diagnostic purposes only.

The population density of the excited state  $n(p)$  can be obtained from the absolutely calibrated line emission:

$$\varepsilon_{pk} = n(p) A_{pk} , \quad (1)$$

$A_{pk}$  is the transition probability from level  $p$  to level  $k$ . The population density  $n(p)$  depends on the plasma parameters, such as  $T_e$ ,  $n_e$  and can be calculated with collisional radiative models which provide coupling coefficients  $R(p)$ :

$$n(p) = n_0 n_e R_0(p) + n_i n_e R_i(p) . \quad (2)$$

$R_0(p)$  and  $R_i(p)$  describe the coupling of the population density to the ground state and the ion, respectively. In most cases, recombination can be neglected. As a consequence the coupling to the ion cancels in equation (2). The combination of equation (1) with equation (2) gives a common formula which combines measured line emission and collisional radiative modelling:

$$\varepsilon_{pk} = n_0 n_e X_{pk}^{\text{eff}}(T_e, n_e, \dots), \quad (3)$$

where  $X_{pk}^{\text{eff}}(T_e, n_e, \dots) = R_0(p) A_{pk}$  represents an effective emission rate coefficient.

Thus, line radiation depends basically on  $n_e$ ,  $T_e$  and particle density. The latter can be determined if  $n_e$  and  $T_e$  are known from other diagnostic techniques such as Langmuir probes. It should be kept in mind that emission spectroscopy yields results averaged over the line of sight.

#### 3.2. Electron density and electron temperature

Electron density and electron temperature can be determined by emission spectroscopy using diagnostic gases. Using line ratios from emission lines of the same gas, the direct dependence on particle density and electron density of the line radiation cancels (equation (3)). The measured line ratio is then directly given by the ratio of the corresponding effective emission rate coefficients. From calculations with collisional radiative models ratios of effective

emission rate coefficients can be identified which depend on  $n_e$  or on  $T_e$  only. The ADAS code package [11] provides collisional radiative models with a very reliable input data base for neutral helium and singly ionised argon. Detailed investigations have shown that in singly ionised argon the line ratio of emission lines at a wavelength of 480 nm and 488 nm is sensitive on  $n_e$  varying a factor of ten in a region of  $n_e = 5 \times 10^{16} - 5 \times 10^{18} \text{ m}^{-3}$ . In addition, for  $2 \text{ eV} < T_e < 10 \text{ eV}$  the dependence of this line ratio on  $T_e$  is very weak and can be neglected. Since this parameter range fits very well to the expected parameters of the negative ion source, the line ratio 480/488 is chosen for  $n_e$  determination. For this purpose small amounts of argon are added to the discharge (typically 15%), the lines are observed readily in the spectra.

A typical ratio which depends on  $T_e$  and less on  $n_e$ , is the ratio of an neutral argon emission line to an emission line of helium, based on the fact that their excitation energy is quite different. Such a diagnostic would require that the two diagnostic gases have to be added to the hydrogen discharges, which may change the discharge itself. Therefore the analysis of absolute line emission of one gas is preferred for  $T_e$  diagnostics. Since the argon content in the discharge is known from the adjusted argon admixture, an emission line of neutral argon is chosen for  $T_e$  diagnostics, in combination with  $n_e$  known from the line ratio method. Here, the argon line at 750 nm is well suited for the analysis, since the dominant excitation path is the ground state excitation and since the excitation rate coefficient is well known [12]. Due to the steep dependence of the rate coefficient on  $T_e$  this method is very sensitive on  $T_e$ .

Figure 2 shows results for  $n_e$  and  $T_e$  obtained in BATMAN. Electron density is roughly a factor 10 higher in the driver (LOS  $\perp$  grid) as parallel to the grid (4 cm distance), increasing almost linear with RF power. As expected, electron temperature is reduced in the extraction region. For deuterium similar results (open circles) as for hydrogen are obtained in the extraction region. However, it appears that the source operates more sufficiently in deuterium than in hydrogen. Although the filling pressure is the same for deuterium and hydrogen, a lower pressure during the discharge is measured for deuterium than for hydrogen. Electron densities are in good agreement with results from Langmuir probe measurements, whereas  $T_e$  is somewhat higher. The analysis of  $T_e$  is based on the assumption of a Maxwellian electron energy distribution in both cases (spectroscopy and Langmuir probe) however the energy

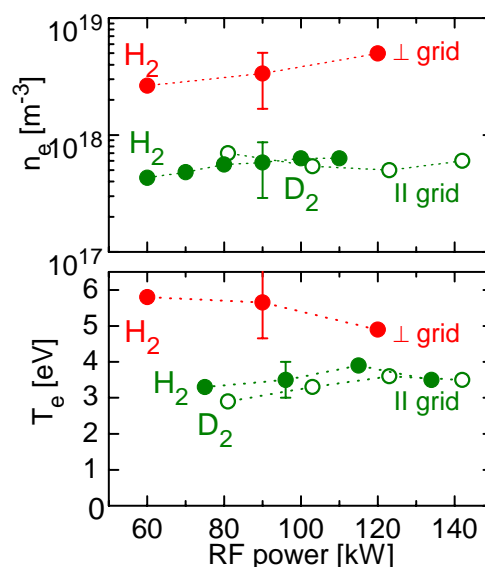


Figure 2. Measured electron density and electron temperature parallel and perpendicular to the plasma grid at a filling pressure of 0.6 Pa in BATMAN (status August 2003). Full circles correspond to hydrogen discharges, open circles to deuterium discharges.

range is different. Emission spectroscopy covers a higher energy part of the EEDF than Langmuir probe measurements. Results from both methods would agree for a bi-Maxwellian EEDF, i.e. a low temperature in the low energy range (0 – approx. 8 eV) followed by a higher temperature. Clarification is expected from further detailed studies with the new Langmuir probe system in rare gas discharges as well as in hydrogen discharges.

### 3.3. Gas temperature and vibrational population of hydrogen

The vibrational population of hydrogen molecules in the ground state is a key parameter in the formation of negative ions by dissociative attachment in the plasma volume. This parameter is obtained from the analysis of vibrational bands of the Fulcher transition [13]. Since this method is sensitive only for the first five vibrational levels in the ground state a vibrational temperature can be assigned to this population. Measurements are carried out in cesium free hydrogen discharges in the extraction region. As shown in figure 3 the vibrational population, i.e.  $T_{\text{vib}}$ , decreases with increasing power, most likely due to the increase of the electron density and therefore enhanced de-population processes by electron collisions. The increase with pressure correlates with a decrease in  $T_e$ . In addition the gas temperature can be obtained from the molecular hydrogen emission [13]. A value of roughly 1500 K is measured which does not depend on input power but slightly on pressure (figure 3). Gas temperature is due to heavy particle collisions whereas the vibrational temperature is due to electron and heavy particle collisions, resulting in quite different absolute values for  $T_{\text{gas}}$  and  $T_{\text{vib}}$ .

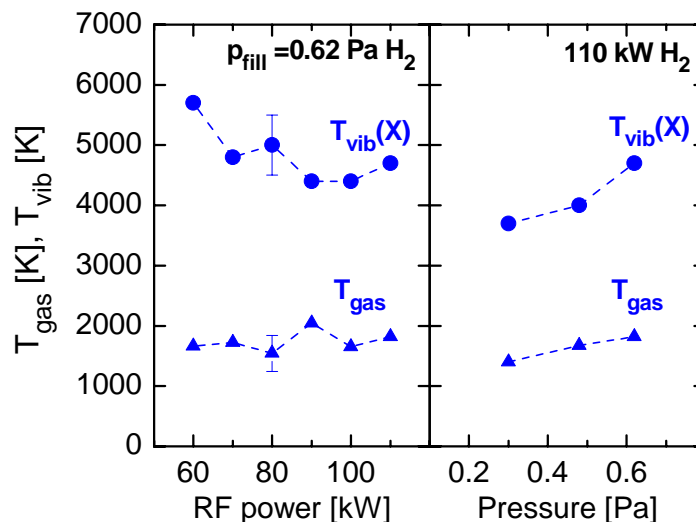


Figure 3. Vibrational temperature of hydrogen molecules and gas temperature in the extraction region of cesium free discharges of BATMAN (status December 2003).

Another quite common method to determine the gas temperature in low pressure plasmas is the admixture of small amounts of nitrogen to the discharge. The analysis of the radiation of nitrogen molecules, in particular the analysis of the rotational structure of vibrational bands of  $\text{N}_2$  or  $\text{N}_2^+$  molecules, yields the rotational temperature which corresponds to the gas temperature [12]. The method was applied to hydrogen discharges in BATMAN. Typical values of  $1200 \text{ K} \pm 300 \text{ K}$  are obtained, being in reasonable agreement with data taken from the analysis of the molecular hydrogen radiation. Measurement of gas temperature is especially important for the determination of gas density and hence the stripping, i.e. the neutralization of the extracted negative ions in the acceleration system (see section 4).

### 3.4. Atomic and molecular hydrogen density

Balmer line emission is correlated with the atomic hydrogen density. Emission of molecular radiation (Fulcher transition) correlates with the molecular density. In an analysis of the line ratio, the direct dependence on electron density cancels. For molecular and atomic hydrogen an improved collision radiative model is available [14] which couples the hydrogen species by population coefficients (equation 2). As obtained from calculations the ratio of the emission rate coefficients for  $H_\gamma$  and Fulcher is almost independent on  $T_e$  and only slightly dependent on  $n_e$ . Thus, the intensity ratio  $H_\gamma/\text{Fulcher}$  is well suited for a determination of density ratios  $H/H_2$ .

Figure 4 shows the density ratios of atomic to molecular hydrogen (full circles) in the driver (LOS  $\perp$  grid) and the extraction region (LOS  $\parallel$  grid, 4 cm distance) of BATMAN at a filling pressure of 0.6 Pa for different RF powers. The density ratio decreases from the driver region to the extraction region and increases slightly with power. The atomic hydrogen particles produced in the driver can recombine at surfaces before they reach the extraction region. Since the electron temperature and electron density is lower in the extraction region as in the driver, the dissociation rate decreases also. The atomic hydrogen density at the grid determines the efficiency of formation of negative ions by the surface effect whereas the molecular hydrogen density is the basis for the formation by the volume mechanism.

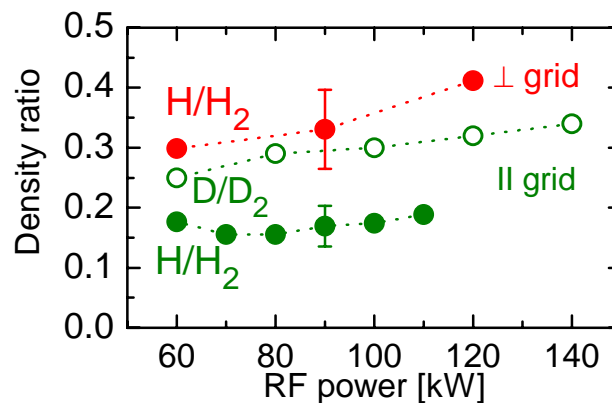


Figure 4. Measured density ratios of atoms to molecules in hydrogen and deuterium parallel and perpendicular to the plasma grid at a filling pressure of 0.6 Pa (BATMAN, Dec. 2003).

In deuterium measurements in the extraction region yield an atomic density which is roughly a factor of 1.5 higher than in hydrogen. This enhancement in the atomic density favours the formation of negative ions by the surface mechanism. The decrease in  $T_e$  (figure 2) reduces the losses by electron stripping, which is very sensitive on  $T_e$ . Thus, more negative ions in deuterium discharges can be expected than in hydrogen discharges for same RF power and filling pressure.

### 3.5. Cesium density

For the diagnostic of cesium in the plasma volume suitable diagnostic lines have been identified and analysis methods have been developed. The resonance lines at 455.5 nm and 852.1 nm are the most intense lines of neutral cesium and, for a quantitative analysis, the corresponding excitation cross sections are known. Since the excitation energy is low (2.70 eV and 1.45 eV, respectively) the dependence of the line intensity on  $T_e$  is very weak. Thus, changes in intensity reflect variation of  $n_e$  and neutral cesium density. Since the ionisation energy ( $E_{\text{ion}} = 3.894$  eV) is comparable with  $T_e$  close to the grid, intense lines at 460.3 nm and at 522.7 nm from singly ionised cesium (CsII, Xe-like,  $E_{\text{ion}} = 25.076$  eV) are present in the

spectra. However, for a quantitative analysis, the corresponding rate coefficients are missing and, due to the relatively high excitation energy of  $\approx 16$  eV, the dependence on  $T_e$  can not be neglected. Here, scaling laws are used to determine Cs ion densities.

Apart from the Cs dynamics, one goal of this measurement is to correlate the Cs signals from the plasma volume with the extracted current density of negative ions since this quantity reflects the efficiency of the surface process. This will help us for the operation of the Cs oven, i.e. to decide if the amount of evaporated Cs is too high or to low. The results and details of the diagnostic itself are reported in [15]. The important results, obtained in BATMAN, where the length of the masked plasma grid contributes with 20% to the line of sight (as indicated in figure 1), will be discussed next.

The neutral density of Cs (typically around some  $10^{14}$  m $^{-3}$ ) 4 cm above the extraction grid is rather low, about 5 order of magnitudes below the neutral atomic hydrogen density. It was estimated from CsII emission (460.3 nm line) that roughly 30 times more ions than neutrals are present. The analysis of Cs particle fluxes from the grid into the plasma results in some  $10^{18}$  particles/m $^2$ /s. Measured densities and fluxes go together when cesium is assumed to be released from the surface by sputtering of plasma particles and penetrates into the plasma where it ionises in a range of a few cm. Enhanced sputtering is observed in deuterium and increases drastically when argon is added to the discharge. Time traces of H $_{\beta}$  and H $_{\gamma}$  demonstrate stable plasma conditions whereas Cs lines increase typically during the discharge, showing also a dependence on the extraction voltage. A direct correlation of Cs emission with the extracted negative ion current density is not observed due to the fact that line intensities reflect the sputtering of cesium whereas  $j_{H^-}$  correlates with the surface process directly, i.e. the Cs coverage of the grid.

Time traces of cesium and the dependence on extraction voltage ( $U_{\text{extr}}$ ) are investigated in detail in the MANITU source, where the size of the grid is much larger (300 cm $^2$ ) and the length contributes to 80% to the LOS parallel the grid. During the plasma only phase (0 – 1 second) the intensity of the Cs line is reproducible and constant. After the onset of the extraction, the Cs line intensity and hence the neutral Cs density in the plasma increases during the pulse depending on the extraction voltage (figure 5). This can be explained by an additional sputtering during the period of beam extraction. The electrical field extracting and accelerating the negative ions from the plasma will also accelerate positive ions from ground

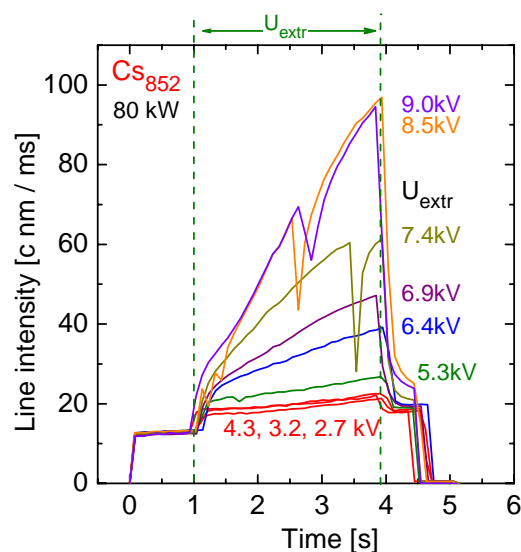


Figure 5. Temporal behaviour of the emission line of neutral cesium at 852 nm in MANITU (80 kW RF power, 0.5 Pa filling pressure) for different extraction voltages ( $U_{\text{extr}}$ ).

potential back into the plasma source. These stream towards the water-cooled backplate of the rectangle source body where cesium condenses. The effect is not so pronounced in BATMAN, where the masked grid has a similar size as the driver, i.e. the ions are accelerated into the driver where cesium deposition is most unlikely. The time constants of the Cs recovery can be seen in the spikes in the time traces which correspond to breakdowns in the voltage system. The high voltage is applied again within 30 ms after the breakdown, whereas cesium requires more time to recover (several 100 ms).

### 3.6. Density of negative ions

A novel diagnostic technique to obtain a line averaged negative ion density is under development and will be described in detail elsewhere [16]. The method is based on the fact that the mutual neutralisation populates dominantly the quantum number  $p=3$  in the hydrogen atom resulting in  $H_\alpha$  radiation (cross sections are given in [17]). As already mentioned in section 3.4, the collisional radiative model for hydrogen is capable of coupling the different hydrogen species. Thus, coupling of  $H^-$  to atomic hydrogen densities by the mutual neutralisation is added. According equation (2), population densities of atomic hydrogen are given by:

$$n_H(p) = n_H n_e R_H(p) + n_{H^+} n_e R_{H^+}(p) + n_{H_2} n_e R_{H_2}(p) + n_{H_2^+} n_e R_{H_2^+}(p) + n_{H^-} n_e R_{H^-}(p) . \quad (4)$$

Recombination (term 2) is efficient only at  $T_e < 1.5$  eV. For atomic to molecular density ratios higher than 0.05 the contribution of dissociative excitation (term 3) can be neglected. The contribution of molecular ions (term 4) is negligible for density ratios  $H_2^+/H < 10^{-2}$  at  $T_e = 5$  eV and  $H_2^+/H < 10^{-4}$  at  $T_e = 2$  eV. For the negative ion sources under investigation equation (4) reduces to the contribution of the atom and the contribution of the negative ion (term 1 and term 5) only. For the mutual neutralisation, i.e. in term 5, the positive ion density is replaced by  $n_e$ .

Since  $H_\alpha$  is most effected by the mutual neutralisation and since all Balmer lines depend on  $n_e$  and  $T_e$ , line ratios are well suited for the analysis of negative ion densities. Figure 6 shows the line ratios calculated with the collisional radiative model as a function of the negative ion density to atomic density for typical electron densities and  $T_e = 3$  eV. The dependence on  $T_e$  is weak in the temperature range  $2 \text{ eV} < T_e < 5 \text{ eV}$ . As can be seen in figure 6, the  $H_\alpha/H_\beta$  ratio is sensitive on the negative ion density whereas the  $H_\beta/H_\gamma$  ratio reflects the plasma parameters,

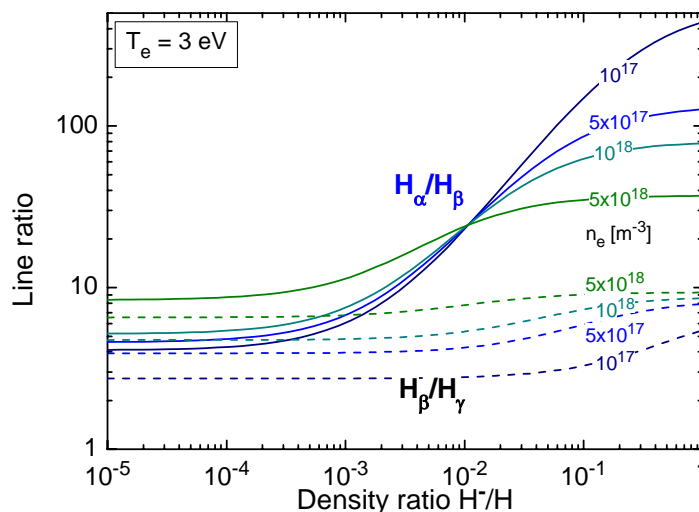


Figure 6. Dependence of Balmer line ratios on the density ratio  $H^-/H$  for different electron densities. The calculations are based on the collisional radiative model for  $H_2$  and  $H$  [14,16].

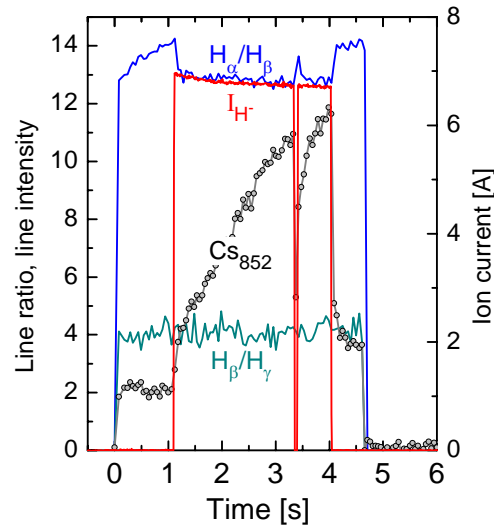


Figure 7. Temporal behaviour of Balmer line ratios  $H_\alpha/H_\beta$  and  $H_\beta/H_\gamma$ , the cesium line at 852 nm, and the extracted current of negative ions at MANITU ( $I_{H^-}$ ).

basically  $n_e$ . Below density ratios of  $H^-/H < 10^{-3}$ , the line ratio is determined by the coupling to the hydrogen atom only. This implies that measured line ratios  $H_\alpha/H_\beta > 4.3$  indicate a line of sight averaged negative ion density in the plasma volume higher than  $10^{16} \text{ m}^{-3}$  for typical parameters of BATMAN and MANITU in the extraction region.

Figure 7 shows time traces of Balmer line ratios and the Cs line obtained parallel to the grid (4 cm distance) in MANITU ( $U_{\text{extr}} = 8 \text{ kV}$ ,  $P_{\text{RF}} = 80 \text{ kW}$ ,  $p_{\text{fill}} = 0.45 \text{ Pa}$ ). A clear dependence on time and in particular a correlation with the extraction is observed in  $H_\alpha/H_\beta$ , whereas  $H_\beta/H_\gamma$  remains constant. The drop in  $H_\alpha/H_\beta$  is caused by the loss of negative ions in 4 cm distance to the grid due to the extraction of the negative ions, indicating a survival length of a few cm. Since surface produced negative ions are extracted, less negative ions reach the observed plasma volume. Converting the line ratios in densities, the negative ion density ranges from 1.1 to  $1.24 \times 10^{17} \text{ m}^{-3}$  during and after extraction. The extracted current of negative ions is also plotted in figure 7 correlating clearly with the  $H_\alpha/H_\beta$  line ratio during the extraction. A further example of the correlation of measured negative ion densities in the

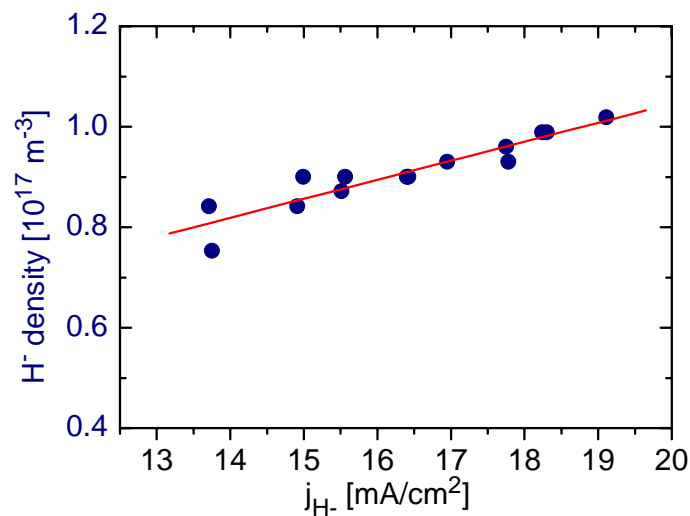


Figure 8. Correlation of negative ion densities in the plasma volume close to the extraction region with the extracted negative ion current density (calorimeter) in MANITU.

plasma volume 4 cm above the grid with extracted current densities (MANITU) is shown in figure 8. Measurements on deuterium discharges yield slightly higher negative ion densities than hydrogen discharges (by a factor of 1.5). This correlates well with the reduced electron temperature and enhanced atomic hydrogen density (section 3.4.).

As mentioned above at BATMAN where the grid size is much smaller than in MANITU, LOS with 4 cm and 1.5 cm distance to the grid are available. Comparing signals obtained at 4 cm distance, the correlation of  $H_\alpha/H_\beta$  ratio and the Cs signal with extracted current densities is less pronounced in BATMAN than in MANITU. However, closer to the grid (1.5 cm distance) the correlation is observed clearly. In addition, the negative ion density is higher close to the grid, being in agreement with one expects for the formation of negative ions by the surface effect.

The fact that the Cs intensity, and thus the amount of cesium in the plasma volume, increases strongly with time but the  $H_\alpha/H_\beta$  line ratio and the extracted ion current show a weak decrease excludes a formation of negative ions based on cesium volume processes.

In figure 7, the maximum of the Cs line emission corresponds to a Cs density of roughly  $10^{15} \text{ m}^{-3}$ . Without Cs, the measured negative ion density decreases to typically  $1 \times 10^{16} \text{ m}^{-3}$  which agrees well with calculated  $H^-$  densities taking into account pure volume production. This measured density results in current densities of  $2 \text{ mA/cm}^2$  and agrees well with measured values ( $2 - 4 \text{ mA/cm}^2$ ) in a cesium free source.

#### 4. Negative ion beam spectroscopy

$H_\alpha$ -beam emission spectroscopy is used to measure the stripping losses, i.e. the neutralization of the extracted negative ions in the extraction system. This leads to non-fully accelerated neutrals reducing the neutral beam power. The energy distribution of the neutrals (neutralization takes place also downstream) can be obtained from the Doppler-shifted  $H_\alpha$  emission. The signal is recorded with a high resolution spectrometer (dispersion of approx.  $0.007 \text{ nm/pixel}$  covering roughly a wavelength range of 7 nm) equipped with 2-dim. CCD camera providing very good measurement of line profiles. The line of sight views the beam approximately 150 cm after the extraction system at a mean angle of 52 degree (beam axis).

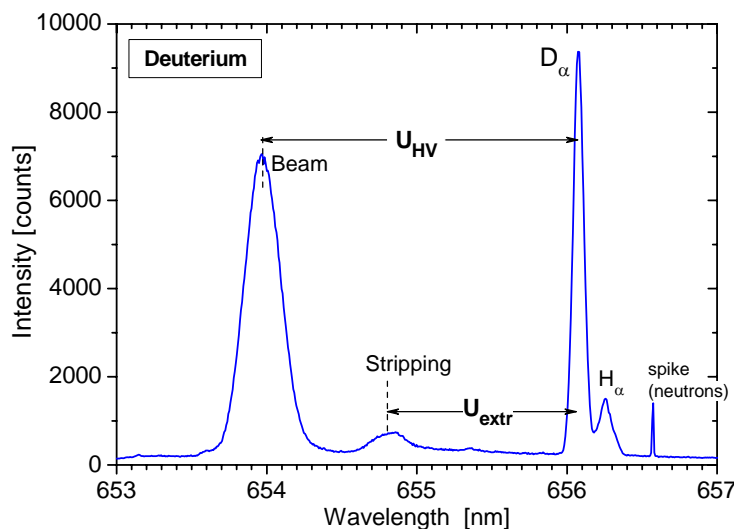


Figure 9.  $H_\alpha$ -beam emission spectroscopy at the negative ion beam of BATMAN where two Doppler shifted peaks appear corresponding to fully accelerated negative ions and non-fully accelerated ions due to electron stripping.

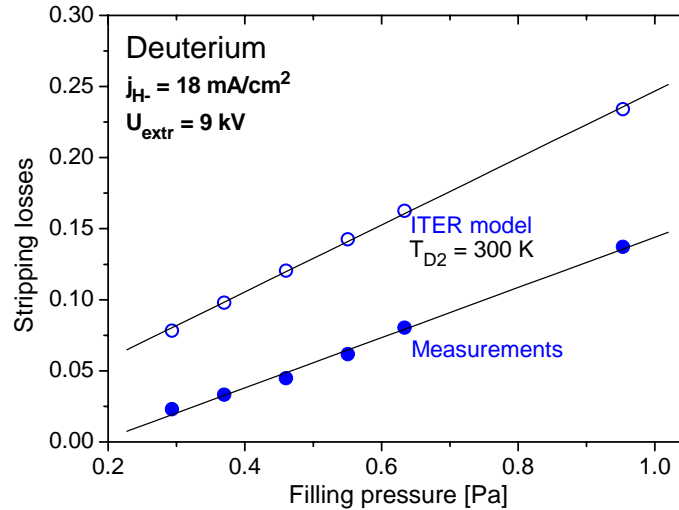


Figure 10. Stripping losses as obtained from  $H_{\alpha}$ -beam emission spectroscopy at the negative ion beam of BATMAN in comparison with results from calculations with a simple model also used for the ITER NBI system.

Due to the final divergence of the beam (some degrees), the peaks are broadened mainly by the angle distribution.

Figure 9 shows a typical spectrum recorded in the negative ion beam of deuterium discharges in BATMAN. Besides the non-shifted  $D_{\alpha}$  line emission caused by dissociation and excitation of the background gas, the Doppler shifted  $D_{\alpha}$  line appears corresponding to the fully accelerated  $D^{-}$  particles. The weak peak in the spectrum reflects the losses by electron stripping in the extraction system. The peak position correlates quite well with the extraction voltage indicating that most of the stripping occurs in the first gap between plasma and extraction grid where the pressure is still high.

The relative amount of non-fully accelerated ions can be calculated from a ratio of the stripping peak with the fully-accelerated peak taking the cross sections for the underlying excitation mechanisms for the ( $H_{\text{fast}} + H_2 \rightarrow H_{\text{fast}}(n=3) + H_2$ , [18]) and the  $H^{-}$  in the LOS ( $H^{-} + H_2 \rightarrow H(n=3)$ , [19]) at the corresponding velocities into account. Results for deuterium obtained from a variation of the filling pressure in BATMAN are given in figure 10. A linear increase is observed, resulting in stripping losses of less than 10% for the standard operating parameters of BATMAN. Comparison with the ITER like model shows that the measured stripping losses are well below the calculations where a gas temperature of 300 K is assumed. This indicates that the gas density is overestimated also in the calculations for the stripping in the ITER accelerator, in accordance with the gas temperature measurements reported above.

## 5. Applications to a filamented arc source

The spectroscopy systems were transferred to the filamented arc source, KAMBOKO type source, at CEA, Cadarache. Plasma parameters based on the same analysis methods were obtained in lines of sight parallel to the grid (at roughly 1 cm distance) and perpendicular to the grid through the source body. Some of the results are already presented in [7,8]. However, for comparison purposes of arc sources and RF sources some of the parameters and main differences will be summarized next.

The compilation of results is carried out for cesiated hydrogen discharges at 45 kW arc power and a pressure of 0.3 Pa. The electron density and electron temperature are determined to be

$5 \times 10^{18} \text{ m}^{-3}$  and 5 eV in the source decreasing to  $2 \times 10^{18} \text{ m}^{-3}$  and 2 eV in the plasma volume parallel the grid. This is in reasonable agreement with Langmuir probe measurements. A gas temperature of  $T_{\text{gas}} = 2000 \text{ K} \pm 300 \text{ K}$  is obtained. This is higher by 25% as the respective values of an RF discharge at 100 kW RF power and 0.5 Pa filling pressure. Electron densities parallel to the grid are higher in arc sources, whereas electron temperature is lower, resulting in a similar destruction rate for negative ions by electron stripping. Higher gas temperatures are measured in arc discharges probably caused by the heated filaments ( $T \approx 2400 \text{ K}$ ). The atomic to molecular density ratio is much higher in arc discharges, being typically 0.6 – 0.7. A density of neutral cesium ranging from  $10^{13} - 10^{14} \text{ m}^{-3}$  is measured, whereas the density of singly ionised cesium is much higher, namely  $10^{16} - 10^{17} \text{ m}^{-3}$ . Typical values for RF discharges are  $10^{14} \text{ m}^{-3}$  (neutral cesium) and  $5 \times 10^{15} \text{ m}^{-3}$  (cesium ions). Thus, the cesium balance is quite different in these sources. Negative ion densities are close to  $10^{17} \text{ m}^{-3}$ , being in the same range as measured in RF discharges. As expected, time traces of  $H_{\alpha}/H_{\beta}$  ratios correlate with extracted current densities but also dependences on arc current and Cs lines are obtained.

One of the major difference in the arc source in comparison to the RF source is the presence of tungsten due to the heated filaments. The tungsten line at 400.9 nm is clearly identified in the spectra. The absolute line emission yields a tungsten density of about  $5 \times 10^{13} - 10^{14} \text{ m}^{-3}$  being comparable to the density of cesium. Thus, tungsten and cesium condense at the surfaces, reducing the efficiency of the surface effect causing an increase in cesium consumption.

## 6. Conclusion

Optical emission spectroscopy is introduced as a powerful diagnostic tool for a variety of plasma parameters being of special importance for the optimisation of negative ion formation ( $\text{H}^-$ ,  $\text{D}^-$ ) in negative ion sources. The diagnostic technique is being used as a standard diagnostic tool for the RF ion sources of the IPP (BATMAN and MANTU). Selected results were shown and have been discussed.

Besides the basic parameters of electron density and electron temperature which determine formation and destruction rates of negative ions by the volume processes, gas temperature, atomic and molecular hydrogen densities, cesium densities and even negative ion densities can be measured routinely. The interaction of atomic hydrogen and cesium is of high relevance for the formation of negative ions by the surface effect. A measurement of these densities was highly desirable and becomes now available. In particular the amount of cesium in the source can be quantified and the consumption of cesium by evaporation can be controlled. A novel non-invasive and flexible diagnostic tool has been developed to measure the negative ion densities in the plasma volume. Correlations with extracted negative ion current densities are clearly observed. Thus, variations of source parameters, as power, pressure or magnetic field configurations, Cs evaporation rate, etc. can be directly linked with the plasma parameters and even with extracted current densities. This is of importance for the new test bed RADI [20]. This testbed is devoted for the optimization of a large size RF source, but due to the lack of a large extraction system, the source performance can only be quantified by the plasma parameters.

Although, emission spectroscopy provides line of sight averaged results, a certain spatial resolution is provided by using several lines of sight. Using the feature of plasma monitoring, the temporal behaviour of plasma parameters is measured, showing the stability and reproducibility of the sources. Of course, an easy task for emission spectroscopy is the

detection of impurities, being very useful in the case of leakages.

The same spectroscopy equipment was transferred to the filamented arc source at CEA (MANTIS testbed). The data obtained rely on the same analysis methods allowing for the first time a direct comparison of the plasma parameters. One of the main differences in these two types of sources is the presence of tungsten in the plasma volume of the arc source. Measured tungsten densities are comparable with cesium densities and it is most likely that cesium layers at the surfaces are covered immediately by tungsten, enhancing the work function which is one of the key parameters for the efficiency of the surface effect.

Applications of  $H_{\alpha}$ -beam emission spectroscopy to the negative ion source BATMAN resulted in the quantification of stripping losses in the extraction system. In comparison with calculation by an ITER model measured stripping losses are well below calculations mainly due to the higher gas temperature in the accelerator system as assumed in the model. This system will be transferred to MANITU, but here spatial resolved spectra can be measured in order to measure the beam homogeneity.

## References

- [1] “ITER Technical Basis”, ITER EDA Documentation Series No. 24, Plant Description Document, Sec. 2.5.1. International Atomic Energy Agency (IAEA), 2002.
- [2] D. Boilson et al., Rev. Sci. Inst. **73** (2002) 1093.
- [3] E. Speth et al., *Overview of the RF source development programme at IPP Garching*, contribution at this conference.
- [4] P. Franzen et al., *Status and plans for the development of an RF negative ion source for ITER NBI*, Proceedings of the 23<sup>rd</sup> SOFT conference, Venice (2004).
- [5] U. Fantz, Contrib. Plasma Phys. **44** (2004) 508.
- [6] U. Fantz, *Atomic and Molecular Emission Spectroscopy in Low Temperature Plasmas Containing Hydrogen and Deuterium*, IPP Report **IPP 10/21** (2002).
- [7] D. Boilson et al., *Characterisation of the ITER model negative ion source*, contribution at this conference.
- [8] R. Hemsworth et al., *Development of the Long Pulse Negative Ion Source for ITER*, Kiev conference 2004.
- [9] W. Kraus, P. Franzen, B. Heinemann, E. Speth, O. Vollmer. Fusion Engineering and Design **56-57** (2001) 499.
- [10] O. Vollmer, B. Heinemann, W. Kraus, P. McNeely, R. Riedl, E. Speth, R. Trainham, R. Wilhelm. Fusion Engineering and Design **56-57** (2001) 465.
- [11] H.P. Summers, ADAS user manual version 2.6, <http://adas.phys.strath.ac.uk>, University of Strathclyde, Glasgow, 2002.
- [12] U. Fantz, *Atomic and Molecular Emission Spectroscopy in Low Temperature Plasmas Containing Hydrogen and Deuterium* IPP Report **IPP 10/21** (2002).
- [13] U. Fantz, B. Heger, Plasma Phys. Control. Fusion **40** (1998) 2023.
- [14] D. Wunderlich, Ph.D. Thesis, University of Augsburg (2004).
- [15] U. Fantz et al., Fusion Engineering and Design, submitted.

- [16] U. Fantz et al., to be published.
- [17] M.J. Eerden et al., Phys. Rev. A **51** (1994) 3362.
- [18] C.F. Barnett (ed.), Atomic Data for Fusion. Volume 1: *Collisions of H, H<sub>2</sub>, He, and Li Atoms and Ions with Atoms and Molecule*, **ORNL-6086** (1990).
- [19] J. Geddes et al., J. Phys. B **14**, (1981) 4837.
- [20] P. Franzen et al., *Status of RADI – a RF source size-scaling experiment towards the ITER*, contribution at this conference.